THE ROYAL SOCIETY

J. R. Soc. Interface (2004) **1**, 35–48
DOI: 10.1098/rsif.2004.0005

Design of biomimetic fibrillar interfaces: 2. Mechanics of enhanced adhesion

C.-Y. Hui[1], N. J. Glassmaker[1,†], T. Tang[1] and A. Jagota[2,‡]

[1]*Department of Theoretical and Applied Mechanics, Cornell University, 212 Kimball Hall, Ithaca, NY 14853, USA*
[2]*DuPont Central Research & Development, Experimental Station, E356/261, Wilmington, DE 19880, USA*

This study addresses the strength and toughness of generic fibrillar structures. We show that the stress σ_c required to pull a fibril out of adhesive contact with a substrate has the form $\sigma_c = \sigma_0\Phi(\chi)$. In this equation, σ_0 is the interfacial strength, $\Phi(\chi)$ is a dimensionless function satisfying $0 \leqslant \Phi(\chi) \leqslant 1$ and χ is a dimensionless parameter that depends on the interfacial properties, as well as the fibril stiffness and radius. Pull-off is flaw sensitive for $\chi \gg 1$, but is *flaw insensitive* for $\chi < 1$. The important parameter χ also controls the stability of a homogeneously deformed non-fibrillar (flat) interface. Using these results, we show that the work to fail a unit area of fibrillar surface can be much higher than the intrinsic work of adhesion for a flat interface of the same material. In addition, we show that cross-sectional fibril dimensions control the pull-off force, which increases with decreasing fibril radius. Finally, an increase in fibril length is shown to increase the work necessary to separate a fibrillar interface.

Besides our calculations involving a single fibril, we study the concept of equal load sharing (ELS) for a perfect interface containing many fibrils. We obtain the practical work of adhesion for an idealized fibrillated interface under equal load sharing. We then analyse the peeling of a fibrillar surface from a rigid substrate and establish a criterion for ELS.

Keywords: fibril; fibrillar adhesion; biological mimic; dry adhesion; equal load sharing; contact mechanics

1. INTRODUCTION

Adhesion in insects, spiders and lizards must satisfy two conflicting requirements. The adherence to a substrate must be strong when the animal wants to secure itself. On the other hand, it must be able to move quickly when necessary, e.g. when pursuing prey or escaping a predator. It has been demonstrated that geckos can adhere to both hydrophilic and hydrophobic surfaces with varying degrees surface roughness. In addition, the fundamental mechanism of adhesion in geckos is reversible and the adhesive forces are believed to be of van der Waals type (see Autumn *et al.* 2000; Autumn *et al.* 2002).

Of particular significance are the fibrillar structures on the feet of these animals. In the case of the beetle *Hemisphaerota cyanea*, each foot has about 60 000 bristles, each with two terminal pads (Eisner & Aneshansley 2000). For the tokay gecko (*Gekko gecko*), each foot has nearly 500 000 bristles or setae (Autumn *et al.* 2000). The number density of setae is about 5000 setae mm^{-2}. Each setae is 30–130 µm in length and contains hundreds of projections terminating in 0.1–0.5 µm spatula shaped pads. Thus, the setae of tokay geckos comprise highly hierarchical structures.

Because of its reliance on van der Waals forces, the ability of geckos to adhere to substrates is primarily controlled by mechanics rather than surface chemistry. Hence, the geometry and material properties of the structure must play a pivotal role in enhancing the adhesion. At first glance, it may seem counterintuitive that a fibrillar interface could be stronger and tougher than a perfectly bonded one, since the fibrils lessen the contact area. This reasoning overlooks several important mechanical effects, as demonstrated by the experiment illustrated in figure 1.

In the experimental sample shown in figure 1, fibrils are introduced midway along one side of a rectangular sheet of poly(vinyl butyral) (PVB; Butacite®, The DuPont Company) by removing the polymer between fibrils. The sheet has height, width and thickness of 30, 30 and 0.76 mm, respectively, while the fibrils have a height h of 10 mm and a width $2a$ of 1.23 mm. The edge of the sheet containing the fibrils is bonded to a glass substrate by heating the substrate to the glass transition temperature of the elastomer. A small crack is introduced at one end of the bond and the sheet

†Author for correspondence (njg22@cornell.edu).
‡Present address: Department of Chemical Engineering, Lehigh University, 111 Research Drive, Iacocca Hall, Bethlehem, PA 18015, USA.

Received 6 February 2004
Accepted 3 June 2004
Published online 7 July 2004

(*a*)

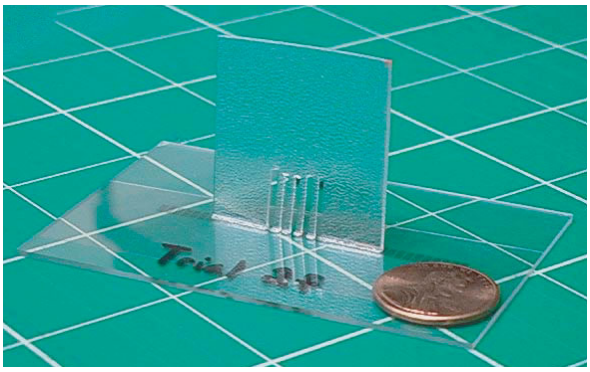

(*b*)

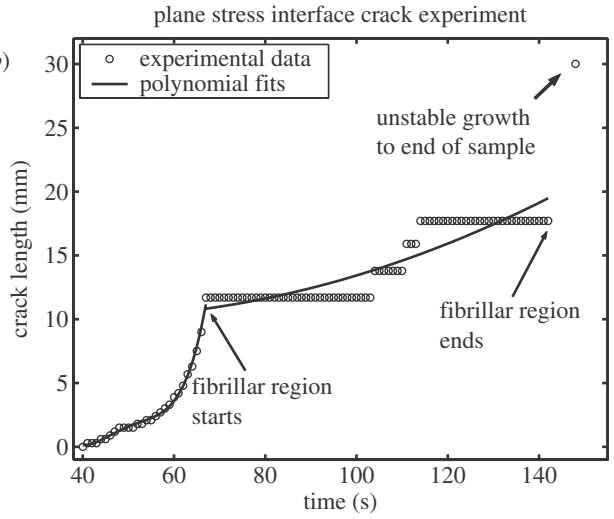

Figure 1. (*a*) PVB sample bonded to glass. (*b*) Crack length as a function of time (equivalently, displacement) for constant rate pull-off of the fibrillar PVB sample.

is pulled upwards by gripping it along the opposite edge. Figure 1 plots the crack length versus time (or, equivalently, displacement, since the gripped edge was pulled at a constant velocity). We see from this figure that the crack starts to accelerate once a critical load or energy release rate is reached. Then the crack is arrested at the first fibril and a substantial stress increase is needed to break that contact. This situation continues until the last fibril is pulled off and crack growth becomes unstable.

This experiment demonstrates that a fibrillar surface can be used as a crack arrester. Most structures contain stress concentrators and/or defects, from which cracks can initiate. Once a crack initiates, it can grow by damaging the material ahead of the crack tip because the stress there is highly concentrated. Indeed, for an infinitely sharp crack in an elastic solid, the crack tip stress field has an inverse square root singularity. For example, the normal component σ_{yy} of the crack tip stress field in the non-fibrillar region of the sheet is

$$\sigma_{yy}(x \to 0) = \frac{K_I}{\sqrt{2\pi x}}, \tag{1.1}$$

where x is the distance of a material point directly ahead of the crack tip. The stress intensity factor K_I is proportional to the applied load and the square root of the crack length. Its precise value depends on the geometry of the sample and can be determined numerically.

Strictly speaking, (1.1) is not valid for an interface crack, unless the elastomer is incompressible and the substrate is rigid. However, these conditions are met approximately in our case, since the bulk modulus of PVB is several orders of magnitude greater than its shear modulus, which is much smaller than the shear modulus of the glass substrate. Figure 2*a* illustrates the situation just before the crack reaches the first fibril. At this instant, the shaded polymer material above the crack face carries no load so that the sharp crack can be replaced by a notch of height h, as shown in figure 2*b*. This abrupt blunting of the crack drastically reduces the stress concentration. Indeed, the crack is no longer a crack! In order for the interface to fail, a crack has to reinitiate from the edge of the fibril (which is a stress concentrator).

As a consequence of crack blunting, the concentrated stress field at the crack tip is redistributed over a zone of length L, which can be significantly greater than the cross-sectional dimensions of the fibril. The load transfer zone length L will be derived later in this work for a peel test. Within this zone, the fibrils are under conditions of *equal load sharing* (ELS). In the ELS scenario, the stress concentration is completely eliminated and the fibrils are subject to a homogeneous state of strain, rather than one in which the deformation of one fibril is coupled to the deformation of nearby fibrils. If all the fibrils in the ELS zone make perfect contact with the substrate and all the contacts have the same strength, then failure of the interface involves a *simultaneous* failure of *all* fibrils inside this zone. This is in contrast to crack propagation, where stress concentration favours a sequential failure of fibrils with the fibril closest to the crack tip failing first.

In addition to the crack arrest behaviour, another advantage of a fibrillar structure was pointed out by the recent work of Jagota & Bennison (2002). For a perfectly bonded non-fibrillar interface, assuming no inelastic deformation, the energy needed to fail a unit area of the interface is the work of adhesion W_{ad}, which for van der Waals solids is of the order of 40–80 mJ m^{-2} (see, e.g. Israelachvili 1992). However, Jagota & Bennison find that the work required to separate a fibrillar surface is much higher, since the elastic strain energy stored in the fibrils is also lost during pull-off. If this stored energy is much higher than W_{ad}, a fibrillar interface will be much tougher.

Actually, a similar idea was first conceived by Lake & Thomas (1967), who noticed that the fracture toughness of elastomers is typically two orders of magnitude higher than the energy required to break a unit area of covalent bonds. They attributed this difference in fracture energy to the following hypothesis: the breaking of a single bond in a chain releases all the stored energy in the chain between cross-links and this energy is much greater than the energy required to break a single bond. Since the energy stored in an elastic fibril is proportional to the square of the pull-off stress, increasing the pull-off stress will have a significant effect on the toughness. However, the pull-off stress is not

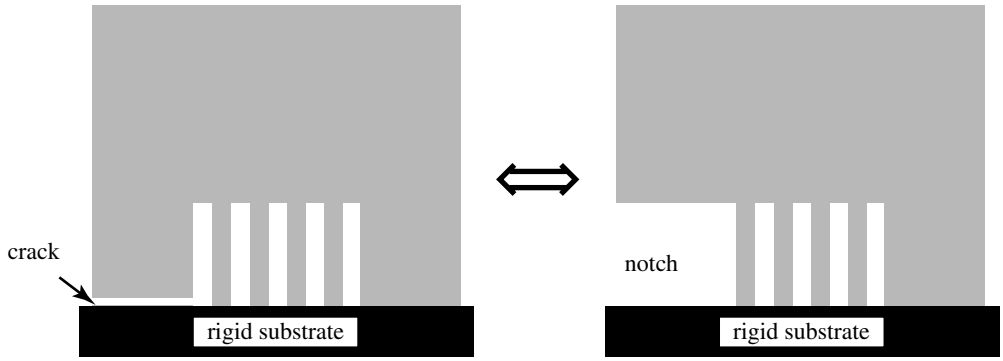

Figure 2. Introducing a fibrillar region converts a sharp crack into a blunted notch with a large process zone. Furthermore, it requires the crack to re-initiate at every fibril–substrate interface.

a material property because the edge of a fibril is a stress concentrator. As we will demonstrate below, the pull-off stress depends on the fibril geometry, material properties and the surface interaction at the fibril–substrate interface.

Several researchers have recently begun to tackle parts of the fibrillar adhesion problem, focusing mostly on explanations of how the biological structures work. Persson (2003) has developed a model for fibrillar contact that includes a description of the adhesive mechanism, as well as arguments for the advantages of a fibrillar system on rough surfaces. Several of his ideas are reinforced with theory and experiments in the companion paper to this one (Glassmaker *et al.* 2004), which also addresses important constraints on fibrillar surface design, i.e. buckling and lateral collapse of fibrils. Finally, Arzt *et al.* (2003) have shown, using the Johnson–Kendall–Roberts (JKR) theory of adhesive contact (see Johnson *et al.* 1971), why setal scale reduction results in increased pull-off force. However, Arzt *et al.* ignore the role of setal structure in enhancing energy loss during decohesion.

The focus of our approach is to provide understanding and design guidelines for synthetic, biologically inspired mimics, the simplest being an array of fibrillar posts protruding from a backing film. Our companion paper (Glassmaker *et al.* 2004) examines how a fibrillar interface achieves maximal contact with its mating surface. As mentioned above, the chief issues there include the flexibility, buckling and lateral collapse of fibrils. This paper presents results on how a fibrillar structure enhances adhesion.

The plan of this paper is as follows. We first determine the stress required to pull off of a *single* fibril. The goal here is to study the dependence of the pull-off stress on fibril geometry, material and surface interaction forces. Knowledge of this pull-off stress allows us to determine the maximum practical work of adhesion of a fibrillar interface based on the assumption of ELS. We then establish the necessary conditions for ELS when a fibrillar structure is subjected to a peel test. Finally, preliminary experimental results on fibrillar poly(dimethlysiloxane) (PDMS) and polyimide samples are compared with the theoretical models.

2. THEORETICAL RESULTS

2.1. Pull-off stress of a single fibril

In this section, we address the question, 'What is the force P_c needed to pull off a cylindrical fibril of radius a attached on one of its ends to a substrate, assuming that there is adhesion between the two surfaces?' We consider two different scenarios: in the first, the fibril is much stiffer than the substrate; in the second, the situation is reversed. In the first case the *local* contact stresses can be modelled by treating the fibril as rigid. The substrate is assumed to be linearly elastic with Young's modulus E_s. For the sake of simplicity, we shall assume that the substrate is an elastomer, with Poisson's ratio $\nu_s \cong 0.5$. In the second case, the fibril is linearly elastic and the substrate is rigid. The Young's modulus of the fibril is denoted by E_f.

The surface interaction at the fibril–substrate interface will be modelled using a cohesive zone model. In this model, the normal stress σ resisting separation of the interface is assumed to be a function of the separation δ between the two surfaces; that is, $\sigma = \Psi(\delta)$, where Ψ has the general form sketched in figure 3*a*. The simplest example is the Dugdale–Barenblatt (DB) model (see Dugdale 1960; Barenblatt 1962), shown in figure 3*b*.

In the DB model, interface separation occurs when σ reaches the interfacial strength σ_0, which is the maximum stress that the interface can withstand. The interface can continue to open until the critical opening δ_c is reached, after which the interface fails since it can no longer support tension. The work of adhesion is the area under the σ versus δ curve. For the DB model, $W_{ad} = \sigma_0 \delta_c$.

Case I: Rigid fibril on elastic substrate ($E_f \gg E_s$). If one assumes the fibril and substrate are perfectly bonded, then the normal component of the stress field on the fibril–substrate interface $z = 0$ is given by Boussinesq (see Johnson *et al.* 1971), i.e.

$$\sigma_{zz}(r) = \frac{P}{2\pi a^2}\left(1 - \frac{r^2}{a^2}\right)^{-1/2}, \quad r < a, \tag{2.1}$$

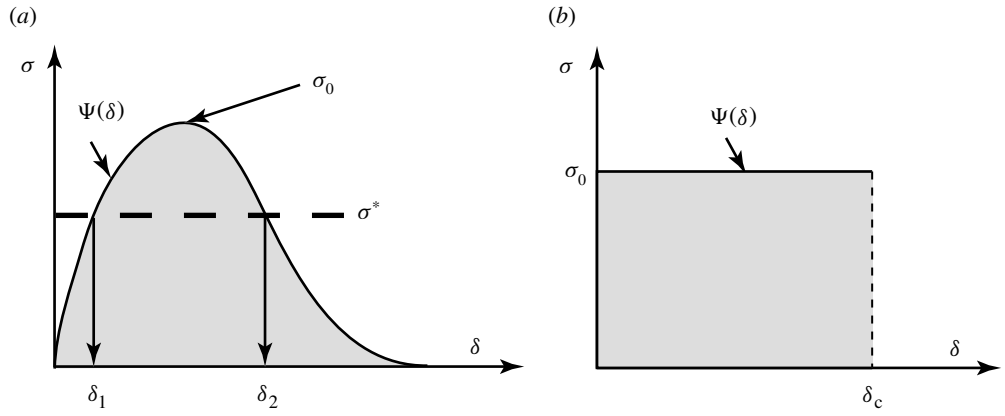

Figure 3. Cohesive zone models. The tensile normal stress $\sigma = \Psi(\delta)$ restrains an interface from separating. The distance separating the two surfaces of the interface is denoted by δ. Note that the work of adhesion is the area under the curve. (a) Cohesive zone model with two homogeneous solutions δ_1 and δ_2 for each $\sigma^* < \sigma_0$, the interface strength. (b) Relation between σ and δ for the DB model. When the separation exceeds δ_c, the interface fails since it cannot bear load.

where r is the distance from the centre of the fibril, P is the normal load on the fibril and $2a$ is its diameter. Notice the stress has an inverse square root singularity at the edge of the fibril. This singularity is characteristic of an interface crack between an incompressible elastic solid and a rigid solid. Indeed, because the fibril is rigid, the region external to fibril can be viewed as an external crack, as illustrated in figures 4b and 4c.

Since the interface cannot support the infinite stresses indicated by (2.1), a cohesive zone develops at the edge of the fibril (see figure 4a). Within the cohesive zone, $c \leqslant r \leqslant a$, there is material separation so that perfect contact occurs only in $r < c$, where c is unknown. According to the DB model, the traction in the cohesive zone is $\sigma_{zz} = \sigma_0$. The modified stress field can be obtained using a solution due to Maugis (1992). For a given fibril radius a, the relation between the contact radius c and the applied load P is found to be

$$P = 2c\sigma_0 \left[\sqrt{a^2 - c^2} + \frac{a^2}{c}\cos^{-1}\frac{c}{a}\right]. \tag{2.2}$$

The critical load P_c for pull-off is determined by the condition $\delta(r = a) = \delta_c$ (see figure 3b), which is

$$\delta_c = \frac{4\sigma_0}{\pi E_s^*}\left[c - a + \sqrt{a^2 - c^2}\cos^{-1}\frac{c}{a}\right], \tag{2.3}$$

where $E^* = E_s/(1 - \nu_s^2) = 4E_s/3$, since the substrate is assumed to be incompressible so that its Poisson's ratio $\nu_s = 1/2$. Eliminating c in (2.2) and (2.3) determines the critical load P_c for pull-off.

Consider the flaw insensitive regime where the cohesive stress dominates. In this regime, $c \to 0$ and (2.2) reduces to

$$P = \sigma_0 \pi a^2, \tag{2.4}$$

as expected. The pull-off condition (2.3) becomes

$$\delta_c = \frac{4\sigma_0 a}{\pi E_s^*}\left[\frac{\pi}{2} - 1\right]. \tag{2.5a}$$

Equation (2.5a) implies that if the dimensionless parameter χ_s defined by

$$\chi_s \equiv \frac{\sigma_0 a}{2\pi E_s^* \delta_c} < \frac{1}{8}\left[\frac{\pi}{2} - 1\right]^{-1} \approx 0.22, \tag{2.5b}$$

then the pull-off condition cannot be satisfied.

The other limit corresponds to pull-off due to crack propagation (the flaw *sensitive* regime). In this regime, the cohesive zone is small compared with the contact region, i.e. $c \to a$ and (2.2) becomes

$$P = 4\sigma_0 a^{3/2}\sqrt{2(a - c)}\,. \tag{2.6}$$

The pull-off criterion (2.3) reduces to

$$\delta_c \approx \frac{4\sigma_0(a - c)}{\pi E_s^*}. \tag{2.7}$$

Thus, the critical stress $\sigma_c \equiv P_c/\pi a^2$ for pull-off is

$$\sigma_c = 4\sqrt{\frac{E_s^* W_{ad}}{2\pi a}}. \tag{2.8}$$

Equation (2.8) shows that, in the fracture or flaw sensitive regime, the critical pull-off stress is inversely proportional to the square root of the fibril radius—a classical fracture mechanics result.

To study the transition from fracture to cohesive-stress-dominated failure, we introduce the dimensionless variable

$$\eta \equiv c/a. \tag{2.9}$$

The average fibril stress $\sigma = P/\pi a^2$ is determined using (2.2), i.e.

$$\sigma = \frac{2\eta\sigma_0}{\pi}\left[\sqrt{1 - \eta^2} + \eta^{-1}\cos^{-1}\eta\right]. \tag{2.10}$$

At pull-off, η is given by the normalized form of equation (2.3), which is

$$\chi_s^{-1} = 8\left[\eta - 1 + \sqrt{1 - \eta^2}\cos^{-1}\eta\right]. \tag{2.11}$$

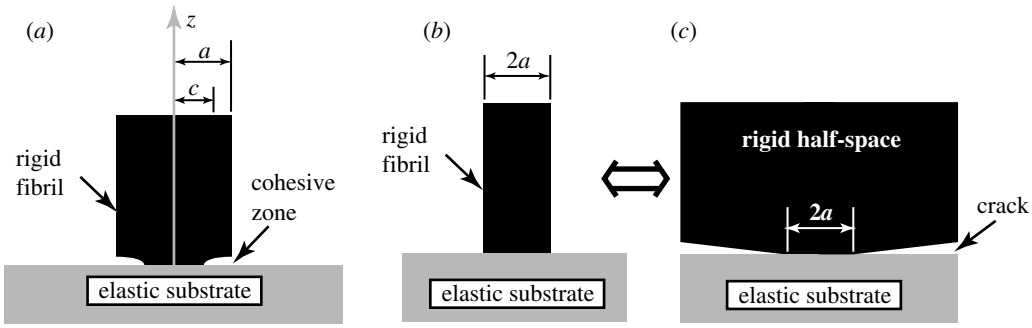

Figure 4. (*a*) During pull-off, a cohesive zone occupies the region $z = 0$, $c < r < a$. (*b*), (*c*) Because the fibril is rigid in comparison with the substrate, the deformation of the substrate is unaffected if material (same as the fibril) is added to the fibril to fill up the upper half-space, provided that an air gap of thickness greater than or equal to δ_c separates the two half-spaces.

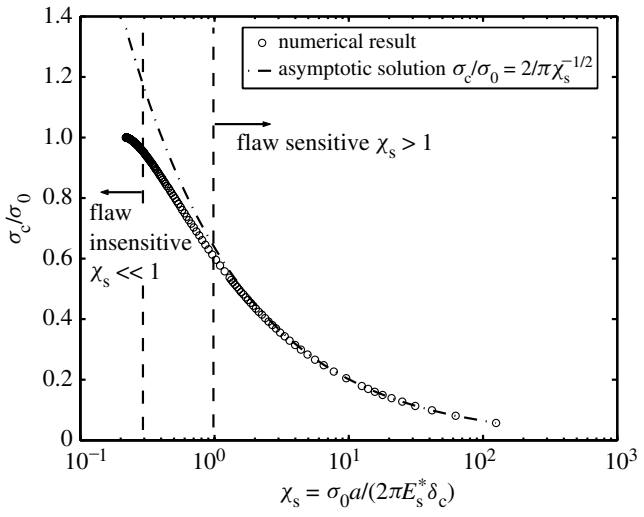

Figure 5. Normalized pull-off stress versus dimensionless parameter $\chi_s \equiv \sigma_0 a/(2\pi E_s^* \delta_c)$ for a rigid fibril on an elastic substrate. The dotted line is equation (2.8) in normalized form.

The critical fibril pull-off stress, σ_c, obtained numerically by eliminating η in (2.10) and (2.11), has the form

$$\sigma_c/\sigma_0 = F(\chi_s). \tag{2.12}$$

The dimensionless function F is plotted in figure 5. The fracture dominated or flaw sensitive regime corresponds to large values of χ_s, i.e. large fibril radius, high cohesive stress and small critical opening and substrate modulus. As expected, the normalized form of (2.8), plotted as a dashed line in figure 5, is correct for large values of χ_s, since the cohesive zone is small in this case. On the other hand, figure 5 shows that, when $\chi_s < 0.3$, the pull-off stress reaches the interfacial strength σ_0, which is the maximum stress the interface can support. Because the critical pull-off stress no longer depends on the size of the fibre when $\chi_s < 0.3$, this regime is called the flaw insensitive regime. To be explicit, failure does not occur by crack propagation in the flaw insensitive regime, since the entire interface must fail at once when the critical stress is equal to the interfacial strength.

Note that the curve in figure 5 terminates at $\chi_s \approx 0.22$, since by (2.5*a*) and (2.5*b*), the pull-off condition cannot be satisfied for $\chi_s < 0.22$. Practically speaking, when $\chi_s < 0.22$, the interface can no longer support further increases in the load on the fibre. This situation is unstable, since any slight increase in fibre load will result in the pull-off of the fibre and loss of equilibrium.

Case II: Elastic fibril on rigid substrate ($E_s \gg E_f$). There is a difference between the first case (rigid fibril, elastic substrate) and the second one. In the first case the pull-off of a fibril can be viewed as the growth of a pre-existing crack as illustrated in figure 4. This does not apply to an elastic fibril since the exterior of an elastic fibril is not an external crack. Indeed, if the interface is frictionless, the edge of the elastic fibril is not even a stress concentrator since the fibril can contract freely there. The worst scenario is when the fibril is perfectly bonded to the substrate (full friction). In this case the stress near the fibril edge has a weaker singularity given by Bogy (1971), i.e.

$$\sigma_{zz}(R \to 0,\ z = 0) = CR^{-\lambda}, \tag{2.13a}$$

where R is the radial distance from the edge and $\lambda \cong 0.4$ for $\nu_f = 0.5$. Linearity and dimensional considerations imply that

$$C = \alpha\sigma a^{\lambda}, \tag{2.13b}$$

where $\sigma \equiv P/\pi a^2$ is the average fibril stress and α is a numerical constant of order one. Since the interface cannot support the infinite stresses indicated by (2.13*a*), a cohesive zone forms at the fibril edge. The failure of this cohesive zone, which occurs first at the edge, leads to crack initiation. Subsequent unstable growth of this crack results in pull-off. The size of the cohesive zone, l_c, can be estimated in the flaw sensitive regime where $l_c \ll a$. To determine l_c, we set $R = l_c$ and $\sigma_{zz} = \sigma_0$ in (2.13*a*); this results in

$$l_c/a = (\alpha\sigma/\sigma_0)^{1/\lambda}. \tag{2.14}$$

A detailed dimensional analysis shows that the normalized average fibril stress to initiate an edge crack

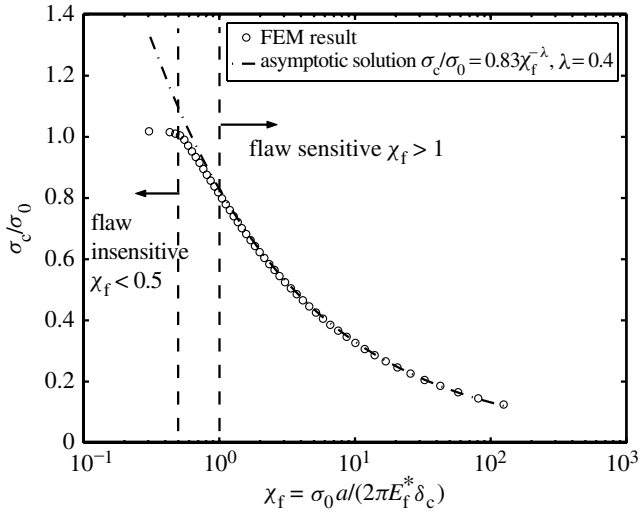

Figure 6. Normalized pull-off stress versus dimensionless parameter $\chi_f \equiv \sigma_0 a/(2\pi E_f^* \delta_c)$ for an elastic fibril on a rigid substrate. The dotted line is equation (2.20), with $B = 0.83$.

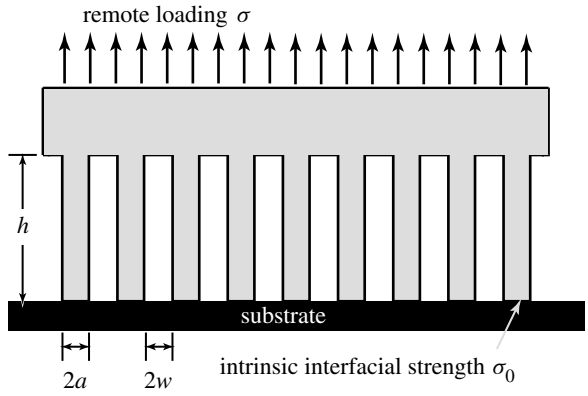

Figure 7. Schematic of a highly idealized scenario where a large number of identical fibrils are in perfect contact with the substrate. The loading is such that all the fibrils are subject to the same load; this condition is called equal load sharing.

$\sigma_{\rm init}/\sigma_0 \equiv P_{\rm init}/(\pi a^2 \sigma_0)$ depends on the single dimensionless constant

$$\chi_f \equiv \frac{\sigma_0 a}{2\pi E_f^* \delta_c}, \tag{2.15a}$$

that is,

$$\sigma_{\rm init}/\sigma_0 = \Phi(\chi_f), \tag{2.15b}$$

where $\Phi(\chi_f)$ is a dimensionless positive function with upper bound equal to 1. Note that χ_f defined by (2.15*a*) is identical to χ_s defined by (2.9), except that the modulus E_s^* in (2.9) is replaced by E_f^*. Details of the solution will be reported elsewhere. Here we summarize the key results. The analysis shows that, once a crack initiates, it becomes unstable and pull-off occurs. Thus, $\sigma_{\rm init} = \sigma_c$, the pull-off stress. In the flaw insensitive regime $l_c \approx a$, $\sigma_c \approx \sigma_0$.

In the flaw sensitive regime $\sigma_c/\sigma_0 \ll 1$ and crack initiation is governed by the edge singularity (2.13). Dimensional considerations show that the opening displacement δ at the edge where $R = 0$ has the form

$$\delta(R=0) = q\frac{l_c \sigma_0}{E_f^*}, \tag{2.16}$$

where q is a numerical constant of order one. Substituting (2.14) into (2.16) gives

$$\delta(R=0) = q\frac{a\sigma_0}{E_f^*}\left(\frac{\alpha\sigma}{\sigma_0}\right)^{1/\lambda}. \tag{2.17}$$

At crack initiation, $\delta = \delta_c$, (2.17) becomes

$$\frac{\sigma_c}{\sigma_0} = B\chi_f^{-\lambda}, \tag{2.18}$$

where $B = \alpha^{-1}(2\pi q)^{-\lambda}$. This analysis shows that, in the flaw sensitive regime, the normalized pull-off stress should scale with $\chi_f^{-\lambda}$, whereas in the flaw insensitive regime $\sigma_c \approx \sigma_0$. These scaling laws are verified by our finite-element results in figure 6, where $\Phi(\chi_f)$ is plotted against χ_f. Equation (2.20), which is the asymptotic result for large χ_f, is plotted in figure 6 as a dashed line. The numerical constant B is found to be 0.83. A comparison of figures 5 and 6 shows that the behaviours of the two curves are very similar, despite the differences in elastic modulus. For example, in the flaw sensitive regime, the pull-off stress is much lower since pull off is controlled by the growth of a crack, due the edge singularity. As for the case of a rigid fibril, pull-off becomes flaw sensitive when $\chi_f > 1$. However, figure 6 shows that flaw insensitivity is valid for a slightly larger range of χ_f for the elastic fibril, i.e. when $\chi_f < 0.5$.

2.2. Energy considerations

In this section we determine the energy required to debond the simple fibrillar structure shown in figure 7. The fibrils in figure 7 are assumed to be circular cylinders identical in length h and diameter $2a$. Let N be the number of fibrils per unit area and let ρ be the area fraction that the fibrils cover, then clearly

$$\rho = N\pi a^2. \tag{2.19}$$

We assume ELS in this section, which would be valid, for example, if the structure in figure 7 is pulled uniformly upwards. The elastic strain energy stored in any fibril is

$$\frac{\sigma^2}{2E_f}\pi a^2 h, \tag{2.20}$$

where σ is the tensile stress on the fibril. This energy is lost during pull-off. In addition to this energy, an amount of work equal to $W_{\rm ad}\pi a^2$ must be supplied to create new surfaces when the interface is opened. Thus, the energy needed to pull off a single fibril is

$$\left(\frac{\sigma_c^2 h}{2E_f} + W_{\rm ad}\right)\pi a^2, \tag{2.21}$$

where σ_c is defined by (2.12) or (2.15*b*).

Equation (2.21) implies that, for a fibrillar interface to be effective as an adhesion enhancer, it is necessary

that

$$\frac{\sigma_c^2 h}{2E_f} \gg W_{ad}. \tag{2.22}$$

To satisfy this condition, and thus increase the toughness of a fibrillar interface, one should decrease the modulus, increase the pull-off stress or increase the fibril length.

From the previous section, it is clear that the maximum pull-off stress is the interfacial strength σ_0. This means that the maximum work to pull off a single fibril is

$$\left(\frac{\sigma_0^2 h}{2E_f} + W_{ad}\right)\pi a^2. \tag{2.23}$$

However, in the flaw sensitive regime, where pull-off is dominated by the edge singularity, the necessary work input to pull off a single fibril depends on whether case I or II above applies. In either case, the work required will be significantly less than the case when $\sigma_c = \sigma_0$. For case I, when the fibril has a much larger modulus than the substrate, using (2.8) in (2.21), one obtains

$$W_{ad}\left(1 + \frac{4E_s^* h}{\pi E_f a}\right)\pi a^2 \tag{2.24}$$

as the work required to pull off a single fibril. Note that, since $E_s/E_f \ll 1$, the quantity inside the parentheses is close to one. In case II, when the substrate has a much larger modulus than the fibril, the work to pull off a single fibril is

$$W_{ad}\left(1 + \frac{\pi B^2}{(1-\nu_f^2)}\frac{h}{a}\chi_f^{1-2\lambda}\right)\pi a^2, \tag{2.25}$$

which results from using equations (2.15*a*) and (2.18) in expression (2.21).

With these results for the work necessary to pull off a *single* fibril in the three limiting cases, we now determine the stress required to pull off a unit area of the fibrillar interface. Assuming all fibrils are in *perfect contact*, the pull-off stress is $\rho\sigma_c$, where σ_c depends on the parameter χ_s or χ_f, as described in the previous section, and ρ is given by equation (2.19). Note that the pull-off stress is the theoretical strength when $\chi_s < 0.3$ or $\chi_f < 0.5$; in these cases $\sigma_c = \rho\sigma_0$. Moreover, the work required to detach a unit area of the interface is

$$W_f = \begin{cases} \rho W_{ad}\left(1 + \dfrac{4E_s^* h}{\pi E_f a}\right), \\ \qquad \chi_s > 1,\ E_f \gg E_s, & (2.26a) \\ \rho W_{ad}\left(1 + \dfrac{\pi B^2}{(1-\nu_f^2)}\dfrac{h}{a}\chi^{1-2\lambda}\right), \\ \qquad \chi_f > 1,\ E_s \gg E_f, & (2.26b) \\ \rho\left(W_{ad} + \dfrac{\sigma_0^2 h}{2E_f}\right), \\ \qquad \chi_s < 0.3 \text{ or } \chi_f < 0.5. & (2.26c) \end{cases}$$

In cases of fibrillar interfaces where adhesion is significantly enhanced compared to their non-fibrillar counterparts, we define a practical work of adhesion W_P by

$$W_P = \rho\left(\frac{\sigma_0^2 h}{2E_f} + W_{ad}\right) \cong \frac{\rho\sigma_0^2 h}{2E_f} \gg W_{ad}. \tag{2.27}$$

Note that the practical work of adhesion is achieved only in cases where $\chi_s < 0.3$ or $\chi_f < 0.5$.

2.3. Stability of a flat interface

The results so far show that, when $\chi_f > 1$, pull-off is flaw sensitive whereas the reverse is true when $\chi_f < 0.5$. What if there were no stress concentration? In this case, it may seem that there should be no length scale affecting the pull-off stress σ_c. If that were the case, one would have $\sigma_c = \sigma_0$, independent of χ_f. We will demonstrate that this is not the case. To eliminate the stress concentration at the fibril edge, consider a frictionless interface. The absence of interfacial shear stresses implies that the normal interfacial stress is uniform. As a result, the fibril is in a homogeneous stress state of pure tension.

In the following, we show that even if the interface is frictionless, the parameter χ_f still plays a key role in determining its stability. Specifically, we show that the homogeneous stress state of the fibril is unstable to perturbations with wavelengths $\lambda > \pi E_f \delta_c/\sigma_0$. This instability is due to the adhesive interaction between the fibril and substrate. If one identifies λ with the fibril radius a, then the condition for instability is $\chi_f > 0.5$. This result shows that $\chi_f > 0.5$ is truly a condition for flaw sensitivity.

Since the stress state of the fibril is homogeneous, one can consider the problem of an infinitely large fibril loaded by uniform tension σ at infinity, as shown in figure 8. The interface is the plane $z = 0$ and the substrate is rigid. To simplify the analysis, we consider plane strain deformation, that is, the out of plane displacement is zero. The adhesive interaction is modelled by the cohesive zone model shown in figure 3*a*, where there are two homogeneous solutions for each value of the applied stress $\sigma = \sigma^*$. Figure 3*a* shows that these homogeneous solutions correspond to uniform interface displacements δ_1 and δ_2, respectively. We will show that the homogeneous equilibrium state with $\sigma = \sigma^*$ and $\delta = \delta_2$ is unstable and will evolve into one of the infinitely many possible equilibrium states illustrated in figure 8*c*. These equilibrium states are possible because the interface model allows solutions in the forms of cracks and cohesive zones that can support normal stress on the interface.

To find the conditions under which the instability occurs, proceed by imposing a small sinusoidal perturbation of the form

$$\delta_p(x,t) = \gamma \sin(2\pi x/\lambda)v(t) \tag{2.28}$$

on the homogeneous equilibrium interfacial displacement δ_2, as shown in figure 8*b*. The magnitude of the perturbation γ is chosen to be infinitesimally small in comparison with the homogeneous interfacial displacement δ_2 and t represents time. The evolution of the unknown function $v(t)$ is determined by the cohesive zone model and the governing equations of linear elasticity. For example, time evolution of the interface can be studied by including a damping term $\beta\dot{\delta}$ in the interface model, i.e.

$$\sigma = \Psi(\delta) + \beta\dot{\delta}, \tag{2.29}$$

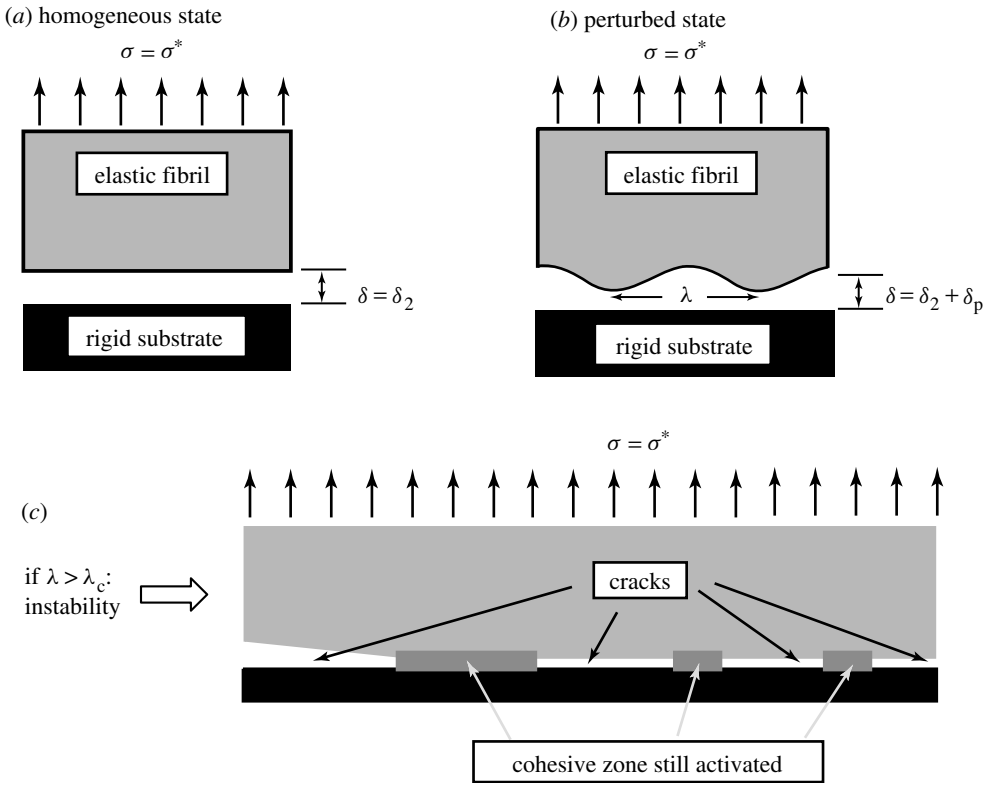

Figure 8. (*a*) An elastic fibril in a state of uniform tension has a homogeneous solution $\delta = \delta_2$, for the cohesive zone model shown in figure 3*a*. Assuming no friction and a perfect interface, this solution is valid for a fibril with infinite diameter. (*b*) Cartoon of the perturbed homogeneous solution. (*c*) The interfacial deformation is unstable when the wavelength of perturbation is substantially large. The instability is due to the interface softening, which allows cracks to develop randomly on the interface. The cracks are separated by cohesive zones.

where $\beta > 0$ is a material constant and $\dot{\delta} \equiv \partial\delta/\partial t$ (see Hui *et al.* (1987) for a more detailed physical interpretation). The behaviour of $\Psi(\delta)$ is shown schematically in figure 3*a*.

The homogeneous equilibrium solution δ_2 satisfies $\sigma^* = \Psi(\delta_2)$ with $\dot{\delta}_2 = 0$. Since the method of analysing the stability of the perturbed elastic fields is analysed by Hui *et al.* (1987), we state the results here without proof. The key result is that the perturbed elastic fields are also sinusoidal, with exactly the same wavelength as in equation (2.28). When using (2.29) as the interface model, the perturbed interfacial displacement $v(t)$ in (2.28) satisfies

$$-\frac{E_{\mathrm{f}}^{*}\pi}{\lambda}v(t) = -Yv(t) + \beta\frac{\mathrm{d}v(t)}{\mathrm{d}t}, \tag{2.30}$$

where $E_{\mathrm{f}}^{*} \equiv E_{\mathrm{f}}/(1-v_{\mathrm{f}}^{2})$ and $Y \equiv -(\partial\Psi/\partial\delta)\big|_{\delta_2} > 0$ (see figure 3*a*). The solution of (2.30) is

$$v(t) = A\exp\left[(-\pi E_{\mathrm{f}}^{*}\lambda^{-1} + Y)\frac{t}{\beta}\right], \tag{2.31}$$

where A is an integration constant. Equation (2.31) shows that the homogeneous solution is unstable if the wavelength of the perturbation exceeds

$$\lambda > \frac{\pi E_{\mathrm{f}}^{*}}{Y}, \tag{2.32}$$

since $v(t)$ grows exponentially when (2.32) is satisfied.

Without specifying a particular form of interface model, the magnitude of Y can be estimated from dimensional considerations, that is

$$Y \equiv \left.\frac{\partial\Psi}{\partial\delta}\right|_{\delta_2} \cong \mathrm{O}\left(\frac{\sigma_0}{\delta_{\mathrm{c}}}\right). \tag{2.33}$$

Thus, according to (2.32), the homogeneous solution becomes unstable when

$$\frac{\pi E_{\mathrm{f}}^{*}}{\lambda} < \frac{\sigma_0}{\delta_{\mathrm{c}}} \quad \text{or} \quad \frac{\lambda\sigma_0}{E_{\mathrm{f}}^{*}\delta_{\mathrm{c}}} > \pi. \tag{2.34}$$

This is analogous to our earlier result $\chi_{\mathrm{f}} > 0.5$ if λ is identified with the fibril radius a.

2.4. Condition for equal load sharing

The results in §§2.2 and 2.3 imply that the maximum stress a fibrillar interface can withstand is $\rho\sigma_0$, where ρ is the area fraction of fibrils. This result gives the maximum practical work of adhesion stated in equation (2.26*c*). To achieve these maximum strength and toughness characteristics, a fibrillar interface must satisfy the condition of ELS; that is, all fibrils must be subject to the same load.

The ELS condition depends on the manner of loading and the geometry of the fibrillated structure. As an illustrative example, consider an adhesive tape fabricated to have a large number of fibrils attached to a flexible backing. Peeling of this tape from a substrate

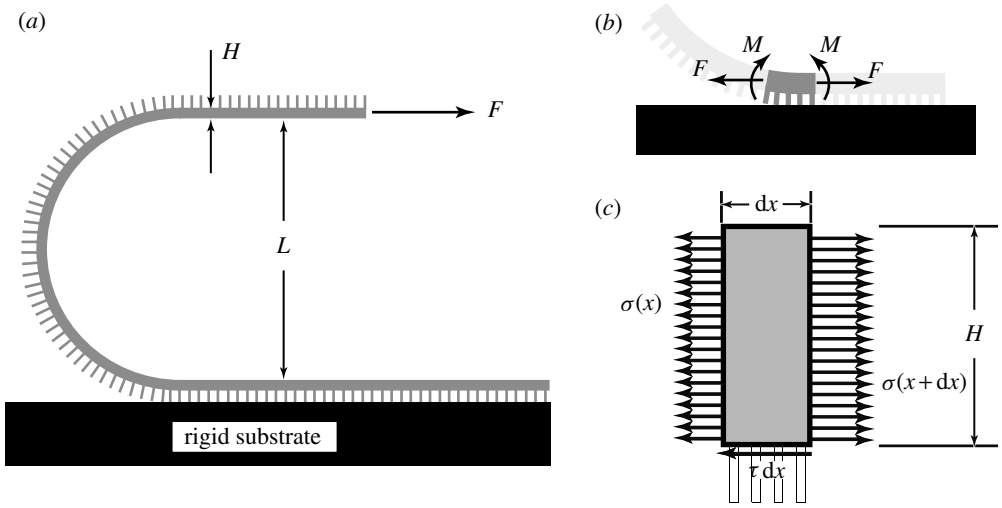

Figure 9. (*a*) Schematic of a 180° peel test of a fibrillated surface from a rigid substrate. (*b*) Free-body diagram of the region near the peel edge. (*c*) Free-body diagram of a section of the fibrillar backing still in contact showing variation of normal stress due to shear on the lower edge.

introduces a stress concentration at the peel edge. In order for the fibrils *near* the peel edge to share the load equally, the characteristic distance of stress decay from the peel edge must be substantially larger than the characteristic fibril spacing $2w$, which is of the order of the fibril radius (see figure 7).

Let us establish the conditions for ELS for a 180° peel test, as shown schematically in figure 9*a*. The backing or peel arm is assumed to be elastic with Young's modulus and Poisson's ratio E_{B} and ν_{B}, respectively. The width of the backing perpendicular to the page is much greater than its thickness, H. This condition implies that the deformation will be independent of the thickness coordinate. The fibrils have identical heights h and radii a and are equally spaced. These dimensions are assumed to be small in comparison with H so that the presence of fibrils has little effect on the deformation of the backing and is confined to a region that is small compared with H. Thus, at distances of order H away from the peel edge, the deformation of the backing can be modelled as an elastica. For a 180° peel test, the relation between L, the peel height and the peel force F per unit width is given by Kendall (1973), i.e.

$$L^2 = 4E^*_{\mathrm{B}} I/F, \tag{2.35}$$

where $I = H^3/12$. Thus, the peel edge is subject to both a moment

$$M = FL = 2\sqrt{E^*_{\mathrm{B}} IF} \tag{2.36}$$

and a horizontal force F.

The elastica solution fails in a small zone near the peel edge, which can be viewed as the tip of a propagating crack. Locally, the deformation of the backing can be modelled as a semi-infinite elastic plate resting on an elastic foundation. The edge of the plate, located at $x = 0$, is subject to a bending moment M and a horizontal force F given by (2.35) and (2.36), respectively. The moment M creates bending whereas the horizontal force F causes shear. The foundation stiffness for bending is determined by the stretching of the fibrils, i.e.

$$k_{\mathrm{B}} = \rho \frac{E_{\mathrm{f}}}{h}. \tag{2.37}$$

The deflection of the backing due to bending, u_z, is governed by

$$E^*_{\mathrm{B}} I \frac{\mathrm{d}^4 u_z}{\mathrm{d}x^4} = -k_{\mathrm{B}} u_z \tag{2.38a}$$

(see Den Hartog (1987) for a derivation). Again, this *linearized* version of the Euler–Bernoulli equation for plate deflection on elastic foundation is valid since we are now considering the local region just to the right of the peel edge (see figure 9*b*). Equation (2.38*a*) is subject to the boundary conditions

$$\left.\begin{aligned} E^*_{\mathrm{B}} I \frac{\mathrm{d}^2 u_z}{\mathrm{d}x^2}\bigg|_{x=0} = -M, \quad \frac{\mathrm{d}u_z}{\mathrm{d}x}\bigg|_{x=0} = 0, \\ u_z(x \to \infty) \to 0. \end{aligned}\right\} \tag{2.38b}$$

The solution of (2.38) is

$$u_z = \frac{M}{\sqrt{E^*_{\mathrm{B}} I k_{\mathrm{B}}}} \mathrm{e}^{-\eta}(\cos\eta + \sin\eta), \tag{2.39}$$

where $\eta = x(4E^*_{\mathrm{B}} I/k_{\mathrm{B}})^{-1/4}$. The characteristic decay distance is $(4E^*_{\mathrm{B}} I/k_{\mathrm{B}})^{1/4} = (E^*_{\mathrm{B}} H^3 h)^{1/4}(3\rho E_{\mathrm{f}})^{-1/4}$. Thus, for ELS to be valid in the bending mode, a necessary condition is

$$\left(\frac{E^*_{\mathrm{B}} H^3 h}{3\rho E_{\mathrm{f}}}\right)^{1/4} \gg a, w. \tag{2.40}$$

For the shearing mode, the ends of the fibrils attached to the backing are subjected to a shear stress τ. Specifically, the shear force acting on a typical fibril in this region is $\pi a^2 \tau/\rho$. This shear force causes a horizontal displacement of the upper edge of the fibril relative to the lower edge, which is attached to the substrate. This horizontal displacement, denoted by u_x, is estimated by treating the fibril as a beam clamped at the lower edge. The relation between the shearing stress

and u_x is found to be

$$\tau = \frac{3\rho E_\mathrm{f} a^2}{4h^3} u_x. \tag{2.41}$$

Thus, the foundation stiffness for the shearing mode is $k_\mathrm{s} = 3\rho E_\mathrm{f} a^2 (4h^3)^{-1}$. A simple force balance of a material element in the backing sheet gives

$$\frac{\mathrm{d}\sigma}{\mathrm{d}x} = \frac{\tau}{H} = \frac{k_\mathrm{s} u_x}{H}, \tag{2.42}$$

where σ is the tension in the backing (see figure 9*b*). Linear elasticity implies that

$$\sigma = E_\mathrm{B} \frac{\mathrm{d}u_x}{\mathrm{d}x}. \tag{2.43}$$

Combining (2.42) and (2.43) gives

$$E_\mathrm{B} \frac{\mathrm{d}^2 u_x}{\mathrm{d}x^2} = \frac{k_\mathrm{s} u_x}{H}. \tag{2.44a}$$

Equation (2.44*a*) is subject to the boundary conditions

$$E_\mathrm{B} \left.\frac{\mathrm{d}u_x}{\mathrm{d}x}\right|_{x=0} = -F/H, \tag{2.44b}$$

$$u_x(x \to \infty) = 0. \tag{2.44c}$$

The solution is

$$u_x = \frac{F}{\sqrt{E_\mathrm{B} k_\mathrm{s} H}} \exp\left(-\sqrt{\frac{k_\mathrm{s}}{E_\mathrm{B} H}}\, x\right). \tag{2.45}$$

Thus, the characteristic stress decay distance in the shear mode is $(4E_\mathrm{B} H h^3)^{1/2} (3E_\mathrm{f} \rho a^2)^{-1/2}$. This result shows that a necessary condition for ELS to occur in the shear mode is

$$\sqrt{\frac{4E_\mathrm{B} H h^3}{3E_\mathrm{f} \rho a^2}} \gg a, w. \tag{2.46}$$

In truly mixed mode loading situations, such as the 180° peel used in this derivation, both (2.40) and (2.46) must be satisfied for ELS to occur near the crack tip. When $H \gg h$, as we have assumed above, satisfaction of (2.46) implies satisfaction of (2.40). However, we have observed empirically in several non-peel experiments that most fibrils fail in tension, implying that the bending mode condition is often sufficient.

The peel force can be determined by enforcing the failure condition

$$u_z(x = 0) = \sigma_0 h / E_\mathrm{f}. \tag{2.47}$$

This condition implies that the fibrils near the peel edge fail at the interface strength, which is valid if ELS holds and the parameter χ_f, from above, is less than 1/2. Then, the peel force is obtained by combining (2.36), (2.37), (2.39) and (2.47), which is

$$F = \frac{\rho \sigma_0^2 h}{4E_\mathrm{f}} = \frac{1}{2} W_\mathrm{P}. \tag{2.48}$$

Note that the peel force is exactly one-half of the practical work of adhesion given by (2.27). This result can also be obtained from an energy balance.

Table 1. Pull-off force for the membrane experiment performed on PDMS samples (circular cross section, $2a = 1\,\mu\mathrm{m}$, $h/2a = 10$). Note that 3 µm fibril spacing is the largest spacing (smallest area fraction ρ) for the samples we fabricated.

Sample	Pull-off force (mN)
Flat control	105
3 µm spacing columns	83

3. EXPERIMENTAL RESULTS

PDMS was moulded into raised columns on a PDMS backing, as described in the companion paper to this one (see Glassmaker *et al.* 2004). Fibrils had circular or square cross sections with 1 µm diameter and sides, respectively. The minimum distance separating fibrils was one, two or three times the fibril's cross-sectional dimension. Fibrils were fabricated with various aspect ratios $h/2a$ ranging from 3 to 10. In another series of experiments, polyimide fibrils with the same dimension ranges were fabricated by direct patterning and deep reactive ion etching of a 10 µm polyimide film on a silicon wafer, as described in Geim *et al.* (2003).

3.1. PDMS samples

We performed two adhesion experiments on the PDMS samples. The first involved compressing an entire sample's fibrillar side ($5 \times 5\,\mathrm{mm}^{-2}$ macroscopic sample size) into contact with a stretched saran® membrane. The flexibility of the saran® membrane allowed slow ramping up of the compressive load. An inverted optical microscope was used to determine when the fibrils came into intimate contact. Once contact was achieved, the sample was pulled off and the maximum tensile force was recorded as a measure of adhesion. The results are shown in Table 1 for circular cross-section fibrils with $h/2a = 10$. The second experiment was to introduce a crack between the structured surface and an opposing adherend. In this case the opposing adherend was a glass cover slip and the crack was introduced by placing a thin wire (12.7 µm diameter) between the sample and glass slip. When the sample and slip are compressed together and released, the length of the non-contact crack region at equilibrium is approximately inversely proportional to the work of adhesion.

The results of the second experiment are shown in figure 10 and Table 2, again for circular cross-section fibrils with $h/2a = 10$. Notice in figure 10 that the wire introduces a well-defined crack length, as the contrast between the contact and non-contact regions is quite distinct. From the data in both Tables 1 and 2, we see that the adhesion of the fibrillar samples is a significant percentage (about 80%) of that for the flat control. This result clearly shows that there is an advantage for adhesion to have fibrils at the interface. In terms of actual area of contact, the fibrillar sample has a *16-fold* increase in work of adhesion ($W_\mathrm{f}/\rho W_\mathrm{ad} = 16$). Based on observations of how the PDMS samples failed during pull-off, we expect them to be in the flaw sensitive fibril pull-off regime, so that equation (2.26*b*) applies.

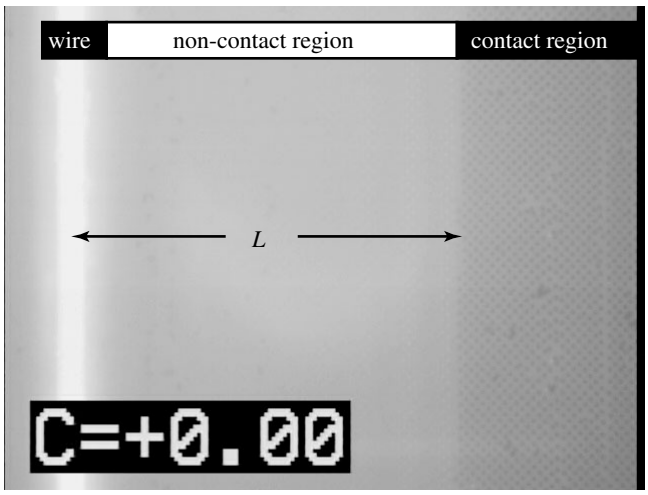

Figure 10. Experiment to determine work of adhesion by inserting a wire at the interface.

Table 2. Crack length for wire crack experiments performed on PDMS samples (circular cross section, $2a = 1\,\mu m$, $h/2a = 10$) adhering to glass.

Sample	Crack length, L (μm)
Flat control	89
3 μm spacing columns	116

The difficulty in applying (2.26*b*) to this experiment is that the cohesive stress σ_0 is unknown.

Israelachvili (1992) states that van der Waals solids may have a cohesive stress as large as 100 MPa. However, the cohesive stress is likely to be much smaller for PDMS because of its low modulus (see Hui *et al.* 2003); a more conservative estimate is $\sigma_0 = 5$ MPa. For the large cohesive stress, (2.26*b*) predicts an adhesion enhancement $W_f/\rho W_{ad}$ of 262, while for the smaller cohesive stress $W_f/\rho W_{ad} = 80$. One way to reconcile the difference between these estimates and the experimental value is to note that (2.26*b*) is derived under the assumption that all fibrils are in perfect contact. In the experiment, however, we observed that this is certainly not the case. In a discussion in the companion paper (Glassmaker *et al.* 2004), it is noted that the presence of imperfect contact significantly decreases the adhesion and hence the pull-off stress. Since the estimates in equation (2.26) are proportional to σ_c^2, the effective adhesion estimate will decrease by an even larger amount.

Whatever theoretical prediction one deems most appropriate, it is evident from the experimental data that the advantage gained by having a fibrillar interface is overwhelmed by loss of contact area for these samples (small ρ in equation (2.26*b*). That is, from Tables 1 and 2, the flat control interface performed better than the fibrillar samples, if one forgets about the difference in actual contact area. It is expected that samples with increased area fraction ρ will perform better than the corresponding flat controls. However, the PDMS samples we made with smaller fibril spacing did not make good contact or adhere well due to lateral collapse (see the companion paper, Glassmaker *et al.* (2004), for more on lateral collapse).

3.2. Polyimide samples

The wire experiment to introduce a crack at the interface was also performed on the polyimide fibrillar samples. However, the adherend for the polyimide samples was a flat sheet of PDMS rather than glass. In figure 11*a* a scanning electron microscope (SEM) micrograph of one of the samples shows well-formed polyimide fibrils with an aspect ratio greater than 5. Figure 11*b* shows results of measured adhesion in this system. Observation of the data in figure 11*b* shows that there is a significant decrease in adhesion energy with increased fibril separation. However, on an actual contact area basis, we again observe an increase in adhesion due to fibril formation. (If the fibrils had no effect on adhesion, W_f/W_{ad} would equal ρ (see equations (2.21) and (2.26)). Figure 11*b* shows that the measured W_f/W_{ad} increases faster than ρ, so that the fibrillar interface enhances adhesion on the basis of actual contact area.) In spite of the slight adhesion increase that we observe, our results differ significantly from those reported by Geim *et al.* (2003) on a very similar system. Specifically, we found that, overall, adhesion was reduced rather than increased for fibrillar interfaces with these dimensions and features, when compared to corresponding flat polyimide control interfaces (see figure 11*b*).

Although our samples and those of Geim *et al.* both consisted of the polyimide fibrils attached to a thin (∼5 μm thick) film of polyimide, one difference is that Geim *et al.* backed the polyimide film with a viscoelastic layer (scotch tape) during adhesion experiments. For the data shown in figure 11*b*, we backed the polyimide film with an approximately 1 mm thick sheet of PDMS, which is nearly ideally elastic. It is possible that some of the additional adhesion energy measured by Geim *et al.* was dissipated in the viscoelastic layer. We repeated experiments on our polyimide film with a double stick viscoelastic tape layer between the polyimide film and PDMS backing. Adhesion was improved by 20% for the flat control interface and by as much as a factor of two for the fibrillar samples, but the adhesion of the fibrillar interface remained significantly lower than that of the flat control.

Although the discrepancy between our results and those of Geim *et al.* (2003) remains unresolved, it is clear that loss of contact area is the most important factor affecting adhesion in our fibrillar polyimide samples. As with the fibrillar PDMS samples, the decrease in overall adhesion due to lost contact area more than offsets any gain due to fibrillar enhancement. To overcome this difficulty, in ongoing work, we seek to increase the area fraction ρ by constructing fibrils with spatula at their ends, again mimicking the natural structure used by geckos (see Autumn *et al.* 2000). Additionally, taking note of our model in equation (2.26), we hope to increase adhesion by making samples with smaller fibrillar diameter and modulus and larger fibrillar height and interfacial strength.

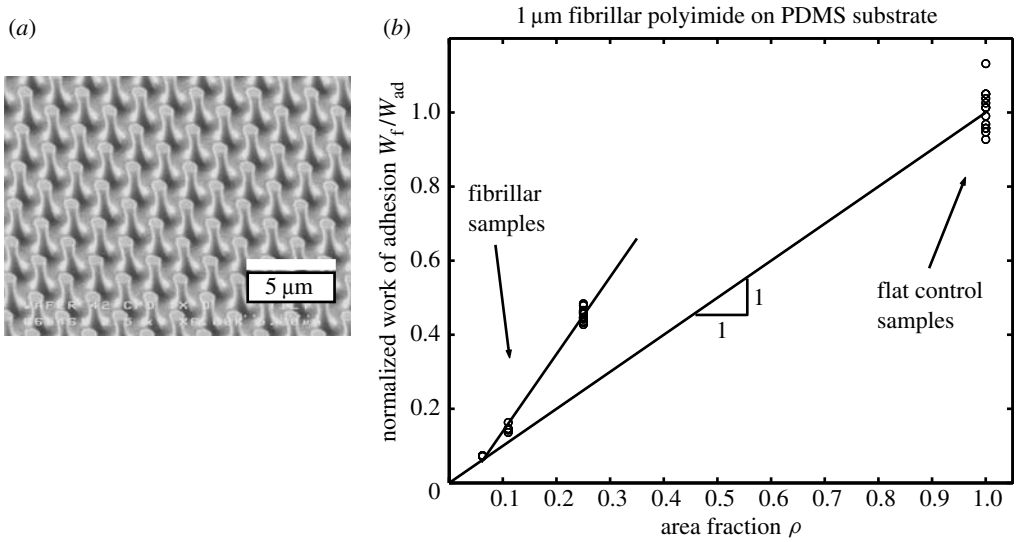

Figure 11. (*a*) SEM micrograph of patterned polyimide. The scale bar is 5 μm. (*b*) Measured work of adhesion decreases linearly with decreasing ρ for the fibrillar samples, as predicted by equation (2.26), but adhesion is enhanced on the basis of actual area of contact (i.e. $W_f/W_{ad} > \rho$). Note that all parameters other than the area fraction (i.e. h, a, E_s^* and E_f) are kept fixed for this set of samples.

4. DISCUSSION

Our results in §§2.1 and 2.2 determine the strength and effective work of adhesion (§2.2, (2.26*a–c*)) of an idealized fibrillar interface. Note that the effective work of adhesion W_f consists of two terms. The first term, ρW_{ad}, is the intrinsic work required to separate two surfaces. The second term in each of (2.26*a–c*) is due to the loss of stored elastic energy in the fibrils. We gave detailed theoretical arguments to support our claim that, to maximize adhesion, fibrils must be designed to satisfy the condition $\chi_s < 0.3$ or $\chi_f < 0.5$. The first condition holds for situations where the fibril is rigid and substrate elastic, while the second holds in the opposite situation.

One way to make the result more general is to introduce an effective modulus, E^*, where $1/E^* \equiv 1/E_f^* + 1/E_s^*$. This definition is consistent with the contact mechanics convention used in the JKR theory (see Johnson *et al.* 1971), and reduces to our results in the proper circumstances. For example, if the substrate is much stiffer than the fibril, $1/E^* = 1/E_f^*$. Conversely, if the substrate is much softer than the fibril, then $1/E^* = 1/E_s^*$. For the DB cohesive zone model, $W_{ad} = \sigma_0 \delta_c$ and the conditions on χ_s and χ_f can be combined into a single condition using the effective modulus E^*, i.e.

$$\chi_{\text{eff}} \equiv \frac{\sigma_0^2 a}{2\pi E^* W_{ad}} \lesssim 1. \tag{4.1}$$

An important assumption we have made throughout our theoretical development is that the fibrils are in perfect contact with the substrate. The assumption that every fibril is in perfect contact with the substrate is practically impossible to achieve, as demonstrated by the experiments in our companion paper (Glassmaker *et al.* 2004). In reality, many fibrils are often in partial contact or are not in contact at all. For example, as mentioned above, Geim *et al.* (2003) showed recently that a fibrillar film of relatively stiff polymer (polyimide) yields enhanced adhesion. However, they note that, in most of their experiments, only a small fraction of the total number of fibrils attained contact.

In experimental systems, surface roughness and the fact that not all fibrils have the same geometrical dimensions (e.g. length) can have a dramatic effect on the force required to pull off a single fibril. Indeed, since the range of van der Waals interactions is at most 10 nm, even the slightest deviation from perfect contact can have a detrimental effect on the pull-off force. As pointed out by the analysis of Persson and Gorb (2003), thin plate-like structures (i.e. spatula) at the terminal ends of setae allow geckos and other animals to achieve better contact on rough surfaces. Because of the important role played by roughness in fibrillar systems, we note that the results in this work give a theoretical upper bound for the strength and work of adhesion of a fibrillar surface.

However, the dimensionless parameter χ_{eff} introduced in this work is of relevance, even to systems not in perfect contact. Specifically, surface roughness in natural and experimental systems generally contains a spectrum of wavelengths and asperity heights. However, a fibrillar structure has sufficient compliance so that the model we have presented, an ideally flat fibril contacting an ideally flat substrate, should be valid, especially at large roughness wavelengths. In the case when the surface is locally non-flat on length scales comparable to the fibril radius, our results and those of JKR theory do not differ greatly. For example, if one assumes that the fibril end is a spherical lens with radius of curvature R in contact with a flat rigid substrate (see, e.g. Arzt *et al.* (2003) and Autumn *et al.* (2002)), then the JKR theory predicts that the pull-off force for a single fibril P_{JKR} is given by

$$P_{\text{JKR}} = 3\pi R W_{ad}/2. \tag{4.2}$$

It is important to note that the JKR theory is based on linear elastic fracture mechanics; that is, the air gap between the surface of a spherical lens and the substrate just outside the contact zone is treated as an external crack. Indeed, in the JKR theory, the normal stress at the edge of the contact zone has an inverse square root singularity. Thus, one can interpret (4.2) as the pull-off force in the flaw sensitive regime. (See figures 5 and 6 and explanations thereof in §2.1.) On the other hand, Maugis (1992) has demonstrated, using a surface interaction model, that there is a regime where the stress concentration is completely eliminated and the surface interaction forces dominate. This regime is the Derjaguin–Muller–Toporov (DMT) limit; in this regime, the pull-off force is

$$P_{\mathrm{DMT}} = 2\pi R W_{\mathrm{ad}}, \tag{4.3}$$

which is 25% higher than the prediction of the JKR theory.

Maugis (1992) showed that the transition from the JKR to the DMT limit depends on the single dimensionless parameter

$$\lambda_{\mathrm{M}} \equiv 2\left(\frac{9R\sigma_0}{16\pi E^*\delta_{\mathrm{c}}}\right)^{1/3}, \tag{4.4}$$

where σ_0 and δ_{c} are the same as those defined in this paper and E^* is the plane-strain Young's modulus of the spherical lens. Maugis showed that large values of λ_{M} correspond to the JKR limit. In addition, the transition from the JKR to the DMT limit occurs at approximately $\lambda_{\mathrm{M}} \approx 1$ or

$$1/9 \approx \frac{R\sigma_0}{2\pi E^*\delta_{\mathrm{c}}}. \tag{4.5}$$

If one identifies R with the fibril radius a, then this condition corresponds to the condition $\chi_{\mathrm{eff}} < 0.1$. Our results in §2.1 are slightly different ($\chi_{\mathrm{s}} < 0.3$ or $\chi_{\mathrm{f}} < 0.5$) because we consider a flat-ended fibril, rather than a spherical lens. Because the two results are nearly identical, we see that the parameter χ_{eff} is just as important when local roughness is a factor as when the surfaces are perfectly flat.

To conclude, we note that the JKR theory will give a reasonable prediction for the pull-off force (and, hence, the work of adhesion) when the diameter of the fibril is large in comparison with the size of the cohesive zone and the radius of curvature of the fibril end is of the order of the fibril radius. However, when χ_{eff} is small, the first condition is violated and the JKR prediction of pull-off force can be substantially flawed. Specifically, note that when the radius of curvature R in equation (4.2) approaches infinity (the limit of a flat-ended fibril), the JKR theory predicts an infinite pull-off force. Thus, for small χ_{eff} and nearly flat-ended fibrils, the theory presented in §2.1 is required to obtain accurate results. (Effectively, our theory is valid when the size of the cohesive zone is small compared with the size of the contact region and when the finite geometry of the sample becomes important. In contrast, the JKR theory assumes that small-scale yielding is satisfied and that the bodies have smooth surface profiles so that the finite geometry can be replaced with a half-space locally.) We note that, for a fixed material and interface model, small χ_{eff} corresponds to small fibril radius, which is precisely the limit of interest in the case of biological fibrillar adhesion and mimics thereof.

5. CONCLUSION

To maximize pull-off stress of a single fibril, it was shown that fibrils must be designed to satisfy the condition $\chi \equiv \sigma_0 a(2\pi E^*\delta_{\mathrm{c}})^{-1} < 1$. This result was obtained for situations where the fibril is rigid and the substrate elastic, but is expected also to hold in cases where fibril and substrate have comparable elastic moduli, as long as one uses the effective modulus E^*, defined by $1/E^* \equiv 1/E_{\mathrm{f}}^* + 1/E_{\mathrm{s}}^*$.

It was demonstrated that choosing $\chi < 1$ is also advantageous from an energy point of view, since fibrillar interfaces with small χ have the largest effective works of adhesion. This line of reasoning relies on the assumptions that elastic energy stored in fibrils is dissipated upon fibril failure, that perfect contact with the substrate is attained and that the fibrils are in a state of equal load sharing when failure occurs. Qualitative arguments and observations were given in support of the first assumption. Quantitative expressions were derived to show when conditions of equal load sharing are satisfied for a common adhesion measurement geometry (180° peel test). Moreover, it was shown in the discussion section that reducing χ increases adhesion, even in rough systems where perfect contact is impossible.

The importance of the parameter χ was emphasized by showing its relation to the wavelength of sinusoidal perturbations that give rise to instabilities in adhering flat interfaces modelled using a cohesive zone force separation law. By equating this wavelength to the fibril radius, the results for maximization of single fibril pull-off stress were verified.

Finally, experimental results for simple fibrillar mimics to biological systems showed enhanced adhesion on a per actual contact area basis and provided partial verification of the theoretical results.

We are grateful for the technical assistance provided by Rick Bender and to Jinsoo Kim for fabricating synthetic PDMS fibrillar samples for indentation measurements. We also acknowledge Nancy Rizzo for gathering all SEM image data included in this paper. Finally, we thank D. Hallahan for helpful discussions regarding the design of synthetic fibrillar systems.

REFERENCES

Arzt, E., Gorb, S. & Spolenak, R. 2003 From micro to nano contacts in biological attachment devices. *Proc. Natl Acad. Sci. USA*, **100**, 10 603–10 606.

Autumn, K., Yiching A., Liang, S., Hsieh, T., Zesch, W., Chan, W. P., Kenny, T. W., Fearing, R. & Full, R. J. 2000 Adhesive force of a single gecko foot-hair. *Nature* **405**, 681–685.

Autumn, K., Sitti, M., Liang, Y. A., Peattie, A. M., Hansen, W. R., Sponberg, S., Kenny, T. W., Fearing, R., Israelachvili, J. N. & Full, R. J. 2002 Evidence for van der Waals adhesion in gecko setae. *Proc. Natl Acad. Sci. USA* **99**, 12 252–12 256.

Barenblatt, G. I. 1962 Mathematical theory of equilibrium cracks in brittle fracture. *Adv. Appl. Mech.* **7**, 55–129.

Bogy, D. B. 1971 Two edge-bonded elastic wedges on different materials and wedge angles under surface tractions. *J. Appl. Mech.* **38**, 377–386.

Den Hartog, J. P. 1987 *Advanced strength of materials*. New York: Dover Publications, Inc., pp. 147–153.

Dugdale, D. S. 1960 Yielding of steel sheets containing slits. *J. Mech. Phys. Solids* **8**, 100–104.

Eisner, T. & Aneshansley, D. J. 2000 Defense by foot adhesion in a beetle (*Hemisphaerota cyanea*). *Proc. Natl Acad. Sci. USA* **97**, 6568–6573.

Geim, A. K., Dubonos, S. V., Grigorieva, I. V., Novoselov, K. S., Zhukov, A. A. & Shapoval, S. Y. 2003 Microfabricated adhesive mimicking gecko foot-hair. *Nature Mater.* **2**, 461–463.

Glassmaker, N. J., Jagota, A., Hui, C. Y. & Kim, J. 2004 Design of biomimetic fibrillar interfaces: 1. Making contact. *J. R. Soc. Interface* (In the press.) (doi:10.1098/rsif.2004.0004).

Hui, C. Y., Logoudas D. C. & Ruina, A. 1987 Constitutive modeling for nontraditional materials. *ASME Appl. Mech. Div.* **85**, 87–116.

Hui, C. Y., Jagota, A., Bennison S. J. & Londono, J. D. 2003 Crack blunting and the strength of soft solids. *Proc. R. Soc. Lond.* A **459**, 1489–1516.

Israelachvili, J. 1992 *Intermolecular and surface forces: with applications to colloidal and biological systems*, 2nd edn. San Diego: Academic Press.

Jagota, A. & Bennison, S. J. 2002 Mechanics of adhesion through a fibrillar microstructure. *Integr. Comp. Biol.* **42**, 1140–1145.

Johnson, K. L., Kendall, K. & Roberts, A. D. 1971 Surface energy and the contact of elastic solids. *Proc. R. Soc. Lond.* A **324**, 301–313.

Kendall, K. 1973 Shapes of peeling solid films. *J. Adhesion* **5**, 105–117.

Lake, G. J. & Thomas, A. G. 1967 The strength of highly elastic materials. *Proc. R. Soc. Lond.* A **300**, 108–119.

Maugis, D. J. 1992 Adhesion of spheres: the JKR–DMT transition using a Dugdale model. *J. Colloid Interf. Sci.* **150**, 243–269.

Persson, B. N. J. 2003 On the mechanism of adhesion in biological systems. *J. Chem. Phys.* **118**, 7614–7621.

Persson, B. N. J. & Gorb, S. 2003 The effect of surface roughness on the adhesion of elastic plates with application to biological systems. *J. Chem. Phys.* **119**, 11 437–11 444.